The Astrophysical Journal, 779:74 (6pp), 2013 December 10 doi:10.1088/0004-637X/779/1/74

SQUEEZING OF PARTICLE DISTRIBUTIONS BY EXPANDING MAGNETIC TURBULENCE AND SPACE WEATHER VARIABILITY

D. Ruffolo[1,2], A. Seripienlert[1,2], P. Tooprakai[2,3], P. Chuychai[2,4], and W. H. Matthaeus[5]
[1] Department of Physics, Faculty of Science, Mahidol University, Bangkok 10400, Thailand; david.ruf@mahidol.ac.th, achara.ser@mahidol.ac.th
[2] Thailand Center of Excellence in Physics, CHE, Ministry of Education, Bangkok 10400, Thailand
[3] Department of Physics, Faculty of Science, Chulalongkorn University, Bangkok 10330, Thailand; paisan@astro.phys.sc.chula.ac.th
[4] School of Science, Mae Fah Luang University, Chiang Rai 57100, Thailand; p.chuychai@sci.mfu.ac.th
[5] Bartol Research Institute and Department of Physics and Astronomy, University of Delaware, Newark, DE 19716, USA; whm@udel.edu
Received 2013 July 19; accepted 2013 September 28; published 2013 November 26

ABSTRACT

Among the space weather effects due to gradual solar storms, greatly enhanced high-energy ion fluxes contribute to radiation damage to satellites, spacecraft, and astronauts and dominate the hazards to air travelers, which motivates examination of the transport of high-energy solar ions to Earth's orbit. Ions of low kinetic energy (up to $\sim$2 MeV nucleon^{-1}) from impulsive solar events exhibit abrupt changes due to filamentation of the magnetic connection from the Sun, indicating that anisotropic, field-aligned magnetic flux tubelike structures persist to Earth's orbit. By employing a corresponding spherical two-component model of Alfvénic (slab) and two-dimensional magnetic fluctuations to trace simulated trajectories in the solar wind, we show that the distribution of high-energy ($E \geqslant 1$ GeV) protons from gradual solar events is squeezed toward magnetic flux structures with a specific polarity because of the conical shape of the flux structures. Conical flux structures and the squeezing of energetic particle distributions should occur in any astrophysical wind or jet with expanding, magnetized, turbulent plasma. This transport phenomenon contributes to event-to-event variability in ground level enhancements of GeV-range ions from solar storms, presenting a fundamental uncertainty in space weather prediction.

Key words: galaxies: jets – ISM: jets and outflows – magnetic fields – solar–terrestrial relations – solar wind – turbulence

1. INTRODUCTION

Turbulence in the expanding solar wind can be examined in situ, and its magnetic fluctuations include quasi two-dimensional (2D) flux structures (Matthaeus et al. 1990; Weygand et al. 2009) similar to flux tubes (Borovsky 2008). Sudden dropouts of low-energy particle fluxes (Mazur et al. 2000; Gosling et al. 2004) are observed from impulsive solar flares, which inject particles over a narrow angular region near the Sun (Reames 1990). Dropouts can be understood in terms of filamentation of the magnetic connection from the injection region due to flux tubelike structures that persist to Earth's orbit (Giacalone et al. 2000; Ruffolo et al. 2003; Zimbardo et al. 2004; Trenchi et al. 2013). However, previous observational and simulation studies have reported a lack of dropouts for ions up to $\sim$2 MeV nucleon^{-1} from gradual solar storms (Mazur et al. 2000), in which particles are injected over a wide volume of space, because there is continuous magnetic connectivity to a very wide source region.

Enhanced fluxes of relativistic solar ions are generally associated with gradual events (Reames 2009). Such ions contribute to space weather effects ranging from satellite and spacecraft damage to health hazards to humans in space (Shea & Smart 2012). Because the lower energy particles that are a major concern in space do not penetrate to aircraft altitudes, relativistic solar ions are the only solar particles of concern for radiation exposure of air travelers and aircraft electronics (Wilson et al. 2003; Lantos 2006). They can also provide the earliest indication of the onset of a space radiation storm (Kuwabara et al. 2006). Thus, their transport to Earth's orbit is of substantial interest. Here we consider protons of 100 MeV to 10 GeV from gradual solar storms and use computer simulations to trace their trajectories in a model of interplanetary magnetic fluctuations. While standard dropout features are indeed absent because of the wide injection region for a gradual event, we have found a novel squeezing of the proton distribution toward higher values of the magnetic potential function for 2D flux structures. Since the potential function of 2D turbulence is generally not known in advance, this represents a basic uncertainty in forecasting of relativistic space radiation levels. Because quasi-2D structures are expected in any magnetized, turbulent plasma (Shebalin et al. 1983; Goldreich & Sridhar 1995), the squeezing effect should apply to other astrophysical winds and jets with expanding magnetic turbulence.

2. MODELING

We have combined various observed properties of solar wind turbulence to develop a new magnetic field model with two-component fluctuations in spherical geometry,

$$\mathbf{B} = \mathbf{B}_0 + \mathbf{b}(\mathbf{r}) = \frac{\mathbf{B}_1 r_1^2}{r^2} + \frac{[\mathbf{b}^{\rm slab}(r) + \mathbf{b}^{\rm 2D}(\varphi, \Lambda)] r_1^2}{r^2}, \quad (1)$$

where $\mathbf{B}_0$ is the radial mean field, which is $\mathbf{B}_1 = B_1 \hat{\mathbf{r}}$ at $r_1 = 1$ AU (at Earth's orbit) with $B_1 = 5$ nT over the region of interest. The slab fluctuation $\mathbf{b}^{\rm slab}$ depends on r, the distance from the solar center, and the 2D fluctuation $\mathbf{b}^{\rm 2D}$ depends on solar longitude φ and latitude Λ. We can write $\mathbf{b}^{\rm 2D}(\varphi, \Lambda) = \nabla \times [a(\varphi, \Lambda)\hat{\mathbf{r}}]$, where a is the magnetic potential function. The fluctuation model is motivated by solar wind observations, including the use of two components (Matthaeus et al. 1990), transverse fluctuations ($\mathbf{b} \perp \mathbf{B}_0$) (Belcher & Davis 1971), a constant amplitude relative to the mean field (Tu et al. 1984), and the specific form $\mathbf{b}^{\rm slab}(r)$ (Saur & Bieber 1999). In addition, a particle transport theory based on 80% 2D and 20% slab turbulent energy was able to explain the mean free path of

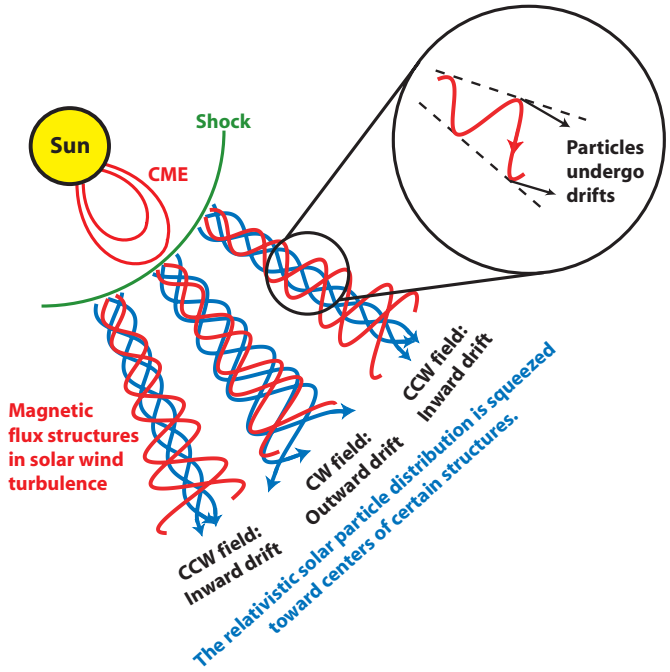

Figure 1. Drift of relativistic solar ions toward certain turbulent flux structures, which can lead to a highly nonuniform distribution in space. A major solar radiation storm involves a coronal mass ejection (CME) that drives a shock (green line), which may accelerate ions to GeV energies, causing significant space weather effects on human activity in space. We show that in the small-scale conical structures of magnetic field lines (red lines) in solar wind turbulence, trajectories of such ions (blue lines) are subject to strong drifts (inset, black arrows) inward for structures with counterclockwise (CCW) magnetic winding and outward from clockwise (CW) structures. The size of the flux structures is exaggerated for clarity; the typical angular width is ∼2°. A relativistic solar particle event typically lasts for a short time, while the Earth is within one structure, so the squeezing of energetic particle distributions toward the centers of CCW structures contributes to event-to-event variability and poses a fundamental uncertainty in space weather prediction.

solar particle transport at low solar latitude (Bieber et al. 1994). We use the radial mean field as an approximation to the Parker spiral field (Parker 1958) because it is difficult to formulate a global 2D fluctuating field for the latter. The radial large-scale field does allow the key transport process of adiabatic focusing (Roelof 1969; Ruffolo 1991). This model does not include a heliospheric current sheet and corresponding reversal of the mean field. We tested including a mean field reversal and found that our conclusions are qualitatively unchanged, so we choose to demonstrate the squeezing effect for the simpler case of a constant mean field. We use a static magnetic field, which is justified because we consider particles moving near the speed of light, which is much greater than the flow speed, sound speed, or Alfvén speed in the solar wind. In generating the 2D field, we use a 2D MHD procedure to properly form coherent structures such as small-scale current sheets (Seripienlert et al. 2010). In any case, our key results are similar for random-phase (Ghilea et al. 2011) or 2D MHD fields, both of which contain magnetic flux structures as illustrated in Figure 1. On the basis of dropout observations (Mazur et al. 2000), we infer that the flux structures typically have an angular width of ∼2°.

The procedure for generating a turbulent magnetic field from the spherical two-component 2D+slab model is as follows. We initially generate the fluctuations in a Cartesian geometry, and use a Kolmogorov power spectrum for turbulence in the inertial range. For the slab component, we use

$$P_{xx}^{\rm slab}(k_z) = P_{yy}^{\rm slab}(k_z) = \frac{C^{\rm slab}}{[1+(k_z\lambda)^2]^{5/6}}, \quad (2)$$

where $C^{\rm slab}$ is the normalization constant for the desired slab fluctuation energy $\langle (b^{\rm slab})^2 \rangle$ and λ is a parallel bendover scale, set to 0.02 AU. For a uniformly spaced set of k_z values, we set $b_j(k_z) \propto \sqrt{P_{jj}(k_z)}e^{i\delta_j(k_z)}$ for a random phase $\delta_j(k_z)$. Then we use an inverse fast Fourier transform to obtain the fluctuating magnetic fields in real space. To convert to a spherical geometry, we identify the z-coordinate with the radius r and use $b_\varphi^{\rm slab}(r) = b_x^{\rm slab}(z)$ and $b_\Lambda^{\rm slab}(r) = b_y^{\rm slab}(z)/\cos\Lambda$, so that $\nabla \cdot \mathbf{b}^{\rm slab} = 0$. In our simulations, we set the box length in the r direction to $L_r = 10{,}000\ \lambda$, and the number of grid points is $N_r = 4{,}194{,}304$. Magnetic field lines and particles are traced only to a few percent of the slab simulation box length in order to avoid periodicity effects (Ghilea et al. 2011).

For the 2D component, we generate a potential function a in terms of the Cartesian coordinates x and y and then map it onto the angular coordinates φ and Λ, respectively, at the reference radius $r_1 = 1$ AU. The potential function $a(x,y)$ is generated in two steps. First, we generate a function $a(k_x, k_y)$ with a random phase at each point in discrete 2D Fourier space for the power spectrum

$$A(k_\perp) = \frac{C^{\rm 2D}}{[1+(k_\perp \ell_\perp)^2]^{7/3}}, \quad (3)$$

where $k_\perp \equiv \sqrt{k_x^2 + k_y^2}$ and $C^{\rm 2D}$ is the normalization constant for the desired 2D fluctuation energy $\langle (b^{\rm 2D})^2 \rangle$. Here we set the perpendicular bendover scale $\ell_\perp$ to 0.033 AU. Then we set $a(k_x, k_y) \propto \sqrt{A(k_\perp)}e^{i\delta(k_x,k_y)}$ for a random phase $\delta(k_x, k_y)$ and perform an inverse fast Fourier transform. In the second step, that random-phase potential is evolved according to a 2D MHD procedure (Seripienlert et al. 2010).

The 2D MHD potential $a(x,y)$ is then recast in terms of heliolongitude $\varphi = x/r_1$ and heliolatitude $\Lambda = y/r_1$, and the resulting function $a(\varphi, \Lambda)$ is used to find the magnetic field as indicated above. In doing so, for a high heliolatitude $|\Lambda|$ the 2D structures become distorted (shortened in longitudinal distance) by a factor of $\cos\Lambda$; thus, we use this procedure only for small values of $|\Lambda|$. In our simulations, we set the box length in the x- and y-directions to $L_x = L_y = 40\lambda$, and the numbers of grid points are $N_x = N_y = 1024$. The ratio of slab energy to 2D energy was 20:80, as suggested by a successful explanation of the mean free path of solar energetic particle (SEP) transport (Bieber et al. 1994). The magnetic fluctuation field was normalized so that the ratio of the root-mean-squared fluctuating field b to B_1 was 0.5. We used an angular region in (φ, Λ) of $50° \times 50°$, centered around the solar equator, with periodic boundary conditions for the magnetic field and for field line and particle trajectories. With a uniform distribution of initial conditions over the entire simulation region and periodic boundary conditions, we can model the very wide injection region for a gradual solar event and also avoid the dropout effects that would result from a concentration gradient.

Particle trajectories were found by solving the Newton–Lorentz equations using a fourth-order Runge–Kutta method with an adaptive step size as documented by Dalena et al. (2012). The initial direction of each particle at $r = 0.1$ AU was parallel to the local magnetic field line in order to represent the effect of strong adiabatic focusing at $r < 0.1$ AU (Ruffolo & Khumlumlert 1995). We also tested assigning a random particle

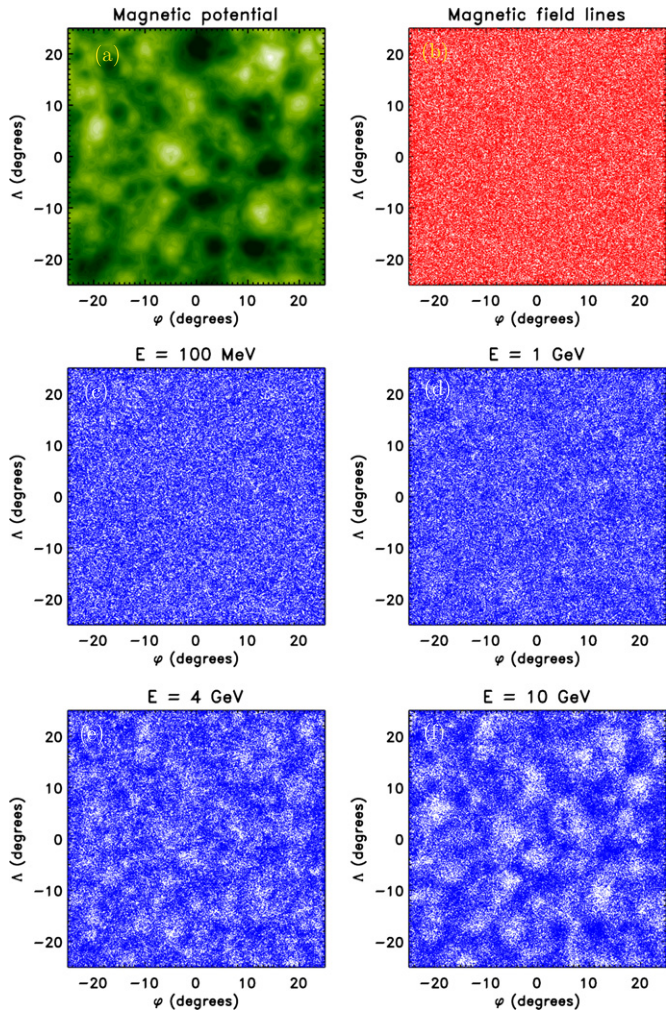

Figure 2. Squeezing of relativistic solar proton distributions into small-scale counterclockwise (CCW) flux structures. (a) Magnetic potential function a vs. solar longitude φ and latitude Λ for a 2D MHD model of the 2D component of interplanetary magnetic turbulence. (b) Magnetic field line locations at Earth's orbit ($r = 1$ AU) as traced from 150,000 uniformly random initial positions at $r = 0.1$ AU from the Sun. (c)–(f) Scatter plots of proton arrival locations at $r = 1$ AU for protons of various energies starting from the same initial locations as the field lines in panel (b). As expected, at $r = 1$ AU the distribution of field lines is uniform, and the distribution of protons of $E = 100$ MeV closely follows that of the field lines. However, for higher energies the drift motion in conical flux structures causes squeezing of the proton distribution toward higher values of the magnetic potential, as found within CCW flux structures. The 10 GeV proton density in panel (f) closely follows the magnetic potential shown in panel (a).

direction up to 30° from the mean field direction and found no noticeable change in the results.

3. DISTRIBUTION OF SOLAR ENERGETIC PARTICLES

We now examine the trajectories of magnetic field lines and particles in a model magnetic field as described above. Figure 2(a) shows a representation of the 2D turbulent magnetic potential $a(\varphi, \Lambda)$, where darker shading corresponds to higher values. We traced 250,000 magnetic field lines and particle trajectories from $r = 0.1$ AU for a uniformly random distribution of initial angular positions over a $50° \times 50°$ region centered at the solar equator. Results for a random subsample of 150,000 are shown in Figures 2(b)–(f). These represent locations of particle acceleration due to a gradual solar event with a coronal mass ejection driving a shock (Figure 1), which can accelerate particles over a very wide angular range (Cane et al. 1991). As expected for this magnetic field model from Liouville's theorem (Ruffolo et al. 2003), the field line distribution remained uniformly random in (φ, Λ) at $r = 1$ AU (Figure 2(b)). We then traced the trajectories of protons of various energies as a function of time t from the same initial locations as the field lines at $t = 0$ and accumulated statistics of particle crossings of the spherical shell $r = 1$ AU for $vt \leqslant 4$ AU, where v is the particle speed, which is constant during propagation through a static magnetic field as used here. There were no noticeable differences between the (φ, Λ) distributions at $r = 1$ AU for different vt intervals, and we considered $vt \leqslant 4$ AU to provide a sufficient time period for accumulation of statistics on promptly arriving particles. The resulting particle-arrival locations at 1 AU are shown in Figures 2(c)–(f). Protons of 100 MeV (or lower) closely follow magnetic field lines, and their distribution is also homogeneous. At 1 GeV, the proton distribution appears slightly nonuniform (Figure 2(d)). Next, we consider a proton energy of 4 GeV, and our results in Figure 2(e) show a novel squeezing effect, where the energetic particles are concentrated into certain regions of (φ, Λ). For 10 GeV protons (Figure 2(f)), the squeezing effect is even stronger, and the particle density appears closely related to the 2D potential function (Figure 2(a)). We obtained similar results for alpha particles of the same gyroradius (i.e., the same momentum per charge), and we expect that they apply to any ion species. For a narrower angular range of proton injection, as for an impulsive solar flare, the squeezing effect also occurs, together with a dropout pattern; however, relativistic protons are usually not observed from impulsive events.

To explain the squeezing effect, we note that in an expanding plasma flow the 2D magnetic flux structures expand with distance to form roughly conical shapes. As illustrated in Figure 1, in a conical magnetic flux tube, the drift motion has a component that systematically brings positive particles inside (outside) a flux surface with **b** that is counterclockwise (clockwise) around a maximum (minimum) of the 2D potential function (Krittinatham & Ruffolo 2009). For negative particles the drift motion is reversed. The deflection is governed by the drift speed relative to the particle speed, which increases with particle momentum, hence the increased squeezing at higher energy in Figure 2. From that figure, we see that the characteristic scale size of the squeezing pattern increases with the particle energy. Apparently, the particles are less sensitive to potential maxima with "catchment basins" smaller than their gyro-orbits, leading to a coarser squeezing pattern at higher energies. Thus, at any given location, the pattern of enhancement or reduction can change with energy, and the energy spectrum of particles at Earth does not necessarily represent the spectrum emitted near the Sun as commonly assumed in data analysis. This is consistent with observations of weak correlation between proton fluxes at $E \sim 10$ MeV and $E \sim 1$ GeV (Gopalswamy et al. 2012). The simulations indicate stronger squeezing at greater distances from the Sun, but they assume r-independent flux structures of 2D turbulence. SEP dropout observations (Mazur et al. 2000; Gosling et al. 2004) indicate that the structures commonly remain intact to $r = 1$ AU; it is not clear as to what distance they survive beyond that.

The squeezing effect is related to the curvature and gradient drifts of particles in conical magnetic flux structures (Figure 1). The standard relativistic formulae for these so-called guiding center drifts (Krittinatham & Ruffolo 2009) are derived by assuming the particle gyroradius to be much smaller than the scales of variation in the magnetic field. The squeezing effect

is essentially the same physical process as guiding center drifts in conical flux structures, but here we will show that it can also occur when the gyroradius is not small compared with the length scales of magnetic field variation. In the remainder of this section, we first apply the standard formulae for guiding center drifts, and then we use a more general Hamiltonian approach that does not assume a small gyroradius.

Consider a particle moving with guiding center speed $v_{||}$ along the field line and gyration speed $v_\perp$. For simplicity, let us demonstrate the effect for $\mathbf{b}^{\rm slab} = 0$ and $\mathbf{b}^{\rm 2D}$ along a conical "flux tube" with azimuthal symmetry, defining a new spherical coordinate system (r, θ', φ') with $\theta' = 0$ along the flux tube axis. Then we use a magnetic field

$$\mathbf{B} = [B_1 \hat{r} + b^{\rm 2D}(\theta')\hat{\varphi}']r_1^2/r^2 \tag{4}$$

and define an aspect angle β by

$$\tan\beta = \frac{b^{\rm 2D}}{B_1}. \tag{5}$$

After some straightforward but laborious calculations of guiding center drifts, we find that the θ'-component of the curvature drift is

$$v_{c,\theta'} = -\frac{\gamma m v_{||}^2}{qB}\left(\frac{\sin\beta}{r} + \cos\beta\frac{\partial\beta}{\partial r}\right) \tag{6}$$

and the θ'-component of the gradient drift is

$$v_{g,\theta'} = \frac{\gamma m v_\perp^2}{qB}\sin\beta\left(-\frac{1}{r} + \frac{\tan\beta}{2}\frac{\partial\beta}{\partial r}\right), \tag{7}$$

where $B = B_0 \sec\beta = B_1(r_1^2/r^2)\sec\beta$. There is strong adiabatic focusing near the Sun, so we expect particles to move nearly parallel to the magnetic field, and most relativistic solar particles are observed to be strongly beamed in interplanetary space near Earth (Bieber et al. 2002, 2013; Ruffolo et al. 2006). Thus, we typically have $v_{||}^2 \gg v_\perp^2$, and we expect the curvature drift to dominate over the gradient drift. Note that in our model, β is constant with r. Then we sum Equations (6) and (7) to obtain a total θ'-drift speed of

$$v_{\theta'} = -\frac{\gamma m v^2}{qB_1 r_1^2}\sin\beta\cos\beta\cdot r, \tag{8}$$

which is directed inward for $q\sin\beta > 0$, e.g., for a positively charged particle in a counterclockwise (CCW) flux structure, and outward for $q\sin\beta < 0$. This is consistent with the squeezing effect seen in simulations, but these formulae for guiding center drifts assume a small gyroradius and may not apply to the GeV-range solar ions considered in this work.

A Hamiltonian approach can also be used to derive the drift velocity. It has the advantages of not requiring a small gyroradius and providing a useful conservation law. In particular, the azimuthal angle φ' is a cyclic variable, so its conjugate momentum $p_{\varphi'}$ is conserved:

$$p_{\varphi'} = \gamma m r^2 \sin^2\theta'\cdot\dot{\varphi}' + qr\sin\theta'\cdot A_{\varphi'} = \text{constant}. \tag{9}$$

The magnetic field (Equation (4)) can be described by a vector potential

$$\mathbf{A}(r,\theta') = A_r(\theta')\hat{r} - \frac{B_1 r_1^2\cot\theta'}{r}\hat{\varphi}, \tag{10}$$

where $b_{\varphi'} = b^{\rm 2D}(\theta') = -(1/r)(\partial A_r/\partial\theta')$. Then we have

$$p_{\varphi'} = \gamma m r^2\sin^2\theta'\cdot\dot{\varphi}' - qB_1 r_1^2\cos\theta' = \text{constant}. \tag{11}$$

This conservation law allows us to infer a simple relationship between θ' and r, after some approximations. Suppose that in the absence of scattering associated with slab turbulence, the particle is highly focused to move nearly parallel to the magnetic field. Then we use a gyro-averaged $v_{\varphi'} = r\sin\theta'\cdot\dot{\varphi}' \approx v\sin\beta$ to obtain

$$p_{\varphi'} = \text{constant} = \gamma m r\sin\theta'\cdot v\sin\beta - qB_1 r_1^2\cos\theta'. \tag{12}$$

We then assume that β is sufficiently small to use $\sin\beta \approx \tan\beta = b^{\rm 2D}(\theta')/B_1$. We further assume that the flux rope interior has

$$b^{\rm 2D} = \pm b\frac{\sin\theta'}{\sin\theta_\perp}, \tag{13}$$

where $\sin\theta_\perp = \lambda_\perp/r$ and $\lambda_\perp$ is a length scale of the 2D turbulence that represents a typical size of 2D structures and is proportional to r. We use the "+" sign for a CCW flux tube and "−" for a clockwise (CW) flux tube. We refer to the value of $\lambda_\perp$ at r_1 as λ_1, so $\sin\theta_\perp = \lambda_1/r_1$. Assuming θ' to be small, we use $\cos\theta' \approx 1 - \sin^2\theta'/2$ to obtain

$$p_{\varphi'} = \text{constant} = \pm\gamma m r\sin\theta'\cdot v\frac{b}{B_1}\frac{r_1\sin\theta'}{\lambda_1} - qB_1 r_1^2\left(1 - \frac{1}{2}\sin^2\theta'\right) \tag{14}$$

$$\sin^2\theta'\left(\frac{1}{2}qB_1 r_1^2 \pm \gamma m v\frac{b}{B_1}\frac{r_1}{\lambda_1}r\right) = \text{constant} \tag{15}$$

$$\sin^{-2}\theta' \propto 1 \pm 2\frac{b}{B_1}\frac{r_{g1}}{\lambda_1}r, \tag{16}$$

where $r_{g1} = \gamma m v/(qB_1)$ is the gyroradius at the location of interest, $r = r_1$. Note, however, that relativistic solar particles often have a low pitch angle, in which case the actual gyro-orbit at the radius of interest may have a much smaller extent than r_{g1}, as will be discussed below. Finally, we can define a twist scale,

$$\lambda_t = \frac{\lambda_1}{2b/B_1}, \tag{17}$$

whose interpretation will be discussed below, and then

$$\sin^{-2}\theta' \propto 1 \pm \frac{r_{g1}}{\lambda_t}\frac{r}{r_1}. \tag{18}$$

Note that the "+" sign, for a CCW flux tube, implies that θ' decreases with radius, whereas the "−" sign, for a CW flux tube, implies that θ' increases with radius. Thus, the equation can explain the squeezing effect seen in simulations of two-component turbulence, with particles drawn inward to CCW flux structures and ejected outward from CW flux structures. This equation is quantitatively consistent with the drift equation (Equation (8)), within the range of validity of the underlying assumptions. The squeezing effect is strong when the second term on the right-hand side of Equation (18) exceeds the first at the radius of interest, $r = r_1$, which is the case when $r_{g1} \geqslant \lambda_t$. This condition determines the energy range above which squeezing is strong at the location of interest.

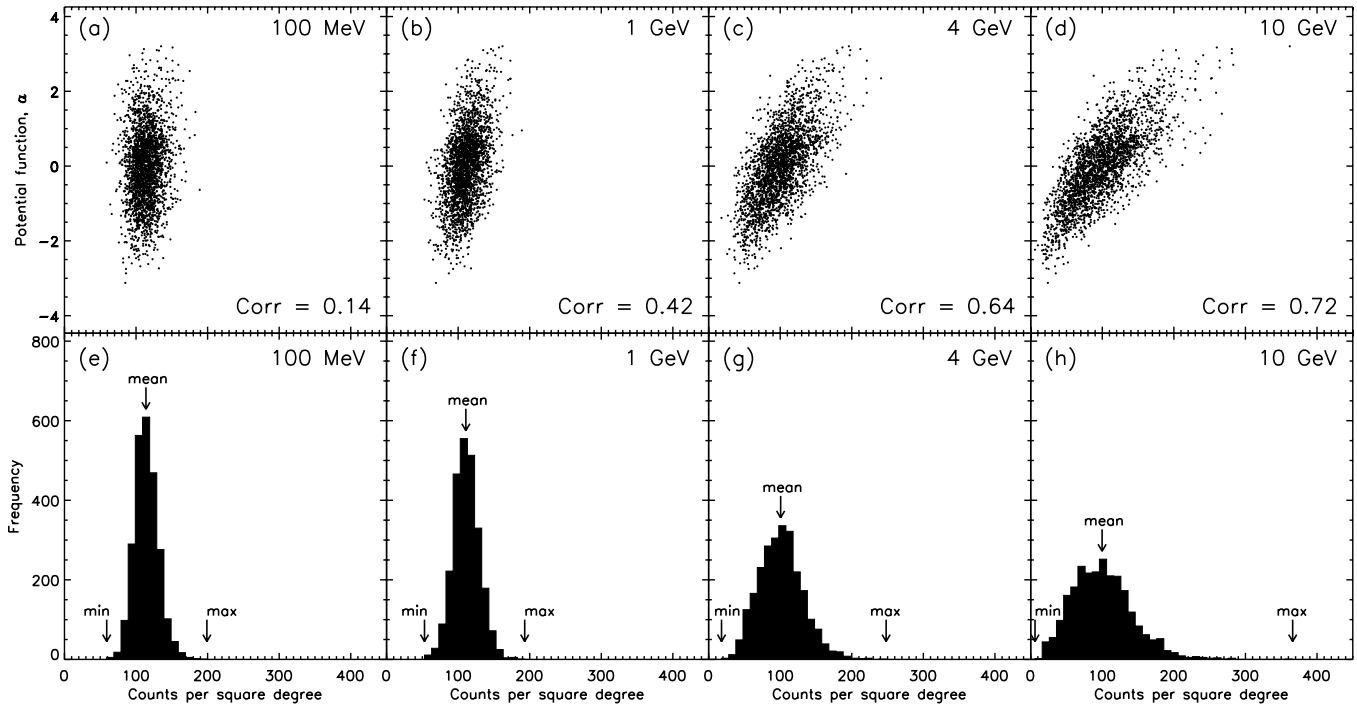

Figure 3. Simulated distribution of relativistic solar proton count rates, showing enhanced variability due to the squeezing effect. (a)–(d) Scatter plots, where each point represents a square-degree box at 1 AU from the Sun, showing the magnetic potential function a in units of $a_{\rm rms}$ as a function of the particle count in that box for various proton energies. (e)–(h) Histograms of particle counts for the same energies. At higher energy, the squeezing effect is stronger, and protons systematically drift to regions of higher a. At 100 MeV, the distribution width is dominated by the simulation's counting statistics, but at $E \geqslant 1$GeV the width greatly increases because of the squeezing effect.

In the context of this derivation for a single flux tube, the scale λ_t represents the perpendicular distance $r \sin\theta'$ where we would find $b^{2D} = B_1/2$, based on the rate of growth of b^{2D} with $\sin\theta'$ as specified by Equation (13). A variation in $\mathbf{b}^{2D}$ of order B_1 implies a substantial twist in the total magnetic field, which is why we call λ_t the twist distance. This actually specifies a rate of change of $\mathbf{b}^{2D}$ with perpendicular distance, so it is not necessary that the flux tube must achieve $b^{2D} = B_1/2$. In other words, the flux tube could be narrower, yet involve sufficiently rapid variation with perpendicular distance that $\lambda_t \leqslant r_{g1}$, in which case the squeezing effect could apply.

Now let us consider the physical limits to the squeezing effect. As noted earlier, our simulations (and derivation) of the squeezing effect assume the persistence of 2D flux structures independent of r. From observations of dropouts (Mazur et al. 2000; Gosling et al. 2004), it is known that many 2D flux structures persist from the Sun to 1 AU. However, such persistence may not actually be a requirement for the squeezing effect. Whatever the 2D structure is, the squeezing can lead to further spatial bunching of the particle distribution.

We note that the squeezing will naturally cease when θ' is so small that the gyro-orbit encompasses the central axis of the flux structure, invalidating our approximation for $v_{\varphi'}$. Now the radius of a gyro-orbit is $r_g \sin\alpha$, where α is the pitch angle between the momentum vector and $\mathbf{B}_0$, and typically relativistic solar particles at Earth are initially concentrated at $\sin\alpha \ll 1$ because of intense adiabatic focusing near the Sun (Bieber et al. 2002; Ruffolo et al. 2006), so $r_g \sin\alpha \ll r_g$. In the absence of scattering, as in the above derivation, the magnetic moment is conserved to a very good approximation. From that approximation, we can derive the angular extent of the gyro-orbit as $r_g \sin\alpha/r \propto \cos^{1/2}\beta \approx 1$, i.e., the angular extent can remain small roughly independently of r. On the other hand, our simulations include slab fluctuations and exhibit some scattering, as does the solar wind. In the presence of pitch angle scattering, the angular extent of the gyro-orbit need not remain constant, and may eventually increase to encompass the axis of the flux structure, after which the squeezing effect is not applicable. Furthermore, as noted earlier with regard to Figure 2, the "catchment basins" of the squeezing effect are apparently wider for increasing particle energy because the larger gyro-orbits are primarily affected by the larger-scale turbulent flux structures.

The twist scale can also be defined for a turbulent magnetic field, though it is based on an approximate description in terms of flux tubes and is therefore not precisely determined. In our simulations of two-component turbulence, we use a root-mean-squared turbulent magnetic field of $b = 0.5B_1$, which is predominantly comprised of 2D fluctuations, so according to Equation (17) we use $\lambda_t = \lambda_1$. To estimate this scale, we consider two viewpoints. According to Section 2, the bendover scale of the 2D turbulence is $\ell_\perp = 0.033$ AU. If this represents the radius of a flux rope with b^{2D} given by Equation (13), then to obtain a root-mean-squared fluctuation of b we need $\lambda_t = \lambda_{c2}/\sqrt{2} = 0.023$ AU. From observations of dropouts (Mazur et al. 2000), the typical size of a flux structure was found to be 0.03 AU, as sampled by random transects of the spacecraft through the structures. Using that value divided by $\sqrt{2}$ yields about $\lambda_t \approx 0.02$ AU. These two estimates are consistent; when we adopt the latter, our expectation that the squeezing effect is strong for $r_{g1} \geqslant \lambda_t$ corresponds to a proton energy range of $E \geqslant 4$ GeV, which is consistent with the simulation results shown in Figure 2.

We note that fundamental processes of turbulence in any magnetized plasma should lead a 2D turbulent cascade with wave vectors perpendicular to the large-scale magnetic field

(Shebalin et al. 1983; Goldreich & Sridhar 1995), so we expect that expanding magnetic turbulence in other astrophysical winds and jets should also exhibit roughly conical flux structures and a similar squeezing effect.

4. IMPLICATIONS FOR SPACE WEATHER VARIABILITY

We also examine variability in the flux of relativistic solar protons due to the squeezing effect. For the proton arrival locations as shown in Figure 2, using the full sample of 250,000 particle trajectories, we determine the distribution of proton counts in each of 2500 square-degree boxes shown in Figure 3. On average, there are ≈100 counts per box. For the lowest energy, 100 MeV, the variability is dominated by statistical counting uncertainty (which would be lower for a detector that observes larger numbers of particles). However, at 1 GeV there is a substantial correlation (0.42) between the count rate and the magnetic potential function a. At $a \approx -3$ we found ≈70–90 counts deg^{-2}, but at $a = 3$ there were 120–160, implying up to two-fold variability due to the squeezing effect, even if it is not visually striking in Figure 2(d). For $E = 4$ GeV and 10 GeV, the squeezing effect is stronger and dramatically enhances the variability of the counting distribution.

Because of space weather effects of solar storms on human activity, there is substantial effort in the community to analyze past solar events and predict SEP fluxes for future events. The strongest space weather effects are associated with ground level enhancements (GLEs), i.e., solar storms that produce high fluxes of relativistic ions above the threshold (≈450 MeV) to shower in Earth's atmosphere and generate signals in ground level detectors (e.g., neutron monitors) above the background level due to galactic cosmic rays (Shea & Smart 2012). In GLE observations, the relativistic solar ion flux typically decays over a few hours (Shea & Smart 2012), during which time the Earth is usually within a single magnetic flux structure; therefore, the variability shown in Figure 3 will be manifest as event-to-event variability. There are known sources of SEP event-to-event variability that are difficult to predict, including the ambient population of "seed" ions (Desai et al. 2003), details of the acceleration process (Tylka & Lee 2006), and transport effects such as the interplanetary magnetic configuration, scattering mean free path, and direction of particle beaming (Bieber et al. 2002; Ruffolo et al. 2006), but these can be analyzed *a posteriori*. In this work we point out the squeezing effect as another strong source of variability in the spectrum and flux of the most energetic solar ions, i.e., the relativistic (GeV-range) ions detected in GLEs. For the foreseeable future, there will be no three-dimensional mapping of the interplanetary magnetic field near Earth over turbulent correlation scales, making it difficult to observationally discern Earth's location with respect to turbulent flux structures of the relevant scales and perform a posteriori analyses of their effects. Thus, we must rely on computer simulations to characterize the effects of squeezing of the relativistic solar particle distribution as a source of uncertainty in the prediction of associated space weather effects.

This research was partially supported by the Thailand Research Fund, a Postdoctoral Fellowship from the Thailand Center of Excellence in Physics, a Research Fellowship from the Faculty of Science, Mahidol University, the U.S. NSF (AGS-1063439 and SHINE AGS-1156094), NASA (Heliophysics Theory NNX08AI47G & NNX11AJ44G), and the Solar Probe Plus/ISIS project.

REFERENCES

Belcher, J. W., & Davis, L., Jr. 1971, JGR, 76, 3534
Bieber, J. W., Clem, J., Evenson, P., et al. 2013, ApJ, 771, 92
Bieber, J. W., Dröge, W., Evenson, P. A., et al. 2002, ApJ, 567, 622
Bieber, J. W., Matthaeus, W. H., Smith, C. W., et al. 1994, ApJ, 420, 294
Borovsky, J. E. 2008, JGR, 113, A08110
Cane, H. V., Reames, D. V., & von Rosenvinge, T. T. 1991, ApJ, 373, 1991
Dalena, S., Chuychai, P., Mace, R. L., et al. 2012, CoPhC, 183, 1974
Desai, M. I., Mason, G. M., Dwyer, J. R., et al. 2003, ApJ, 588, 1149
Ghilea, M. C., Ruffolo, D., Chuychai, P., et al. 2011, ApJ, 741, 16
Giacalone, J., Jokipii, J. R., & Mazur, J. E. 2000, ApJL, 532, L75
Goldreich, P., & Sridhar, S. 1995, ApJ, 438, 763
Gopalswamy, N., Xie, H., Yashiro, S., et al. 2012, SSRv, 171, 23
Gosling, J. T., Skoug, R. M., McComas, D. J., & Mazur, J. E. 2004, ApJ, 614, 412
Krittinatham, W., & Ruffolo, D. 2009, ApJ, 704, 831
Kuwabara, T., Bieber, J. W., Clem, J., Evenson, P., & Pyle, R. 2006, SpWea, 4, S10001
Lantos, P. 2006, Radiat. Prot. Dosim., 118, 363
Matthaeus, W. H., Goldstein, M. L., & Roberts, D. A. 1990, JGR, 95, 20673
Mazur, J. E., Mason, G. M., Dwyer, J. R., et al. 2000, ApJL, 532, L79
Parker, E. N. 1958, ApJ, 128, 664
Reames, D. V. 1990, ApJL, 358, L63
Reames, D. V. 2009, ApJ, 693, 812
Roelof, E. C. 1969, in Lectures in High Energy Astrophysics, ed. H. Ögelmann & J. R. Wayland (NASA SP-199; Washington, DC: NASA), 111
Ruffolo, D. 1991, ApJ, 382, 688
Ruffolo, D., & Khumlumlert, T. 1995, GeoRL, 22, 2073
Ruffolo, D., Matthaeus, W. H., & Chuychai, P. 2003, ApJL, 597, L169
Ruffolo, D., Tooprakai, P., Rujiwarodom, R., et al. 2006, ApJ, 639, 1186
Saur, J., & Bieber, J. W. 1999, JGR, 104, 9975
Seripienlert, A., Ruffolo, D., Matthaeus, W. H., & Chuychai, P. 2010, ApJ, 711, 980
Shea, M. A., & Smart, D. F. 2012, SSRv, 171, 161
Shebalin, J. V., Matthaeus, W. H., & Montgomery, D. 1983, JPlPh, 29, 525
Trenchi, L., Bruno, R., Telloni, D., et al. 2013, ApJ, 770, 11
Tu, C.-Y., Pu, Z.-Y., & Wei, F.-S. 1984, JGR, 89, 9695
Tylka, A. J., & Lee, M. A. 2006, ApJ, 646, 1319
Weygand, J. M., Matthaeus, W. H., Dasso, S., et al. 2009, JGR, 114, A07213
Wilson, J. W., Goldhagen, P., Rafnsson, V., et al. 2003, AdSpR, 32, 3
Zimbardo, G., Pommois, P., & Veltri, P. 2004, JGR, 109, A02113